PAPER   *Special Section on Cryptography and Information Security*

A Dental Radiograph Recognition System Using Phase-Only Correlation for Human Identification

Koichi ITO[†a)], *Member*, **Akira NIKAIDO**[†], *Nonmember*, **Takafumi AOKI**[†], *Member*, **Eiko KOSUGE**[††], **Ryota KAWAMATA**[††], *and* **Isamu KASHIMA**[††], *Nonmembers*

SUMMARY   In mass disasters such as earthquakes, fire disasters, tsunami, and terrorism, dental records have been used for identifying victims due to their processing time and accuracy. The greater the number of victims, the more time the identification tasks require, since a manual comparison between the dental radiograph records is done by forensic experts. Addressing this problem, this paper presents an efficient dental radiograph recognition system using Phase-Only Correlation (POC) for human identification. The use of phase components in 2D (two-dimensional) discrete Fourier transforms of dental radiograph images makes possible to achieve highly robust image registration and recognition. Experimental evaluation using a set of dental radiographs indicates that the proposed system exhibits efficient recognition performance for low-quality images.
key words: *dental biometrics, dental radiograph, image registration, image matching, phase-only correlation, biometrics*

1.   Introduction

Reliable identification of humans is an important topic in commercial, civilian and forensic applications [1]. Traditional approaches for human identification suffer from the disadvantages: passwords and PIN (Personal Identification Number) may be forgotten, and keys, ID card, and passport may be lost, stolen, forgotten, or misplaced. Biometric authentication refers to automatic recognition of individuals based on their physiological or behavioral characteristics such as face, fingerprint, iris, keystroke, signature, voice, gait, etc. Biometrics-based approaches are more reliable than traditional approaches, since biometric traits cannot be lost, forgotten, stolen and misplaced. Among many biometric techniques, this paper focuses on human identification using dental features, which is called *dental biometrics* [2].

The conventional biometric traits, e.g., fingerprint, iris, etc., may not be available when identifying victims of large-scale disasters, e.g., earthquakes, fire disasters, tsunami, terrorism, etc. On the other hand, dental features are one of few biometric traits which can be used for identifying deceased individuals. Dental radiographs have been used as the most common forms of dental records for human identification. Figure 1 shows an example of dental radiograph,

Fig. 1   Example of dental radiograph, which is a periapical image around molars.

which is a periapical image around molars. The purpose of human identification using dental radiographs is to match an unidentified individual's postmortem (PM) radiographs against a set of identified antemortem (AM) radiographs. In forensic odontology, which is also called forensic dentistry, a manual comparison between the AM and PM radiographs is done by forensic experts. Since this task is extremely time consuming, the demand for the automated dental identification system has increased [3].

Previous works of the automated dental radiograph identification system use the contours of the teeth and the shapes of the dental work to compare between the AM and PM dental images [2]–[4]. One of the difficult problems in feature-based approach is that matching performance is significantly influenced by the image quality of radiographs. In many cases, the contours of the teeth can not be extracted from the dental radiograph accurately, since the dental radiograph is often blurred due to substantial noise, poor lighting, etc.

This paper presents a dental radiograph recognition system using Phase-Only Correlation (POC) — an image matching technique using the phase components in 2D Discrete Fourier Transforms (DFTs) of given images. The technique has been successfully applied to sub-pixel image registration tasks for computer vision applications [5]–[7]. In our previous work [8], we have proposed a fingerprint recognition algorithm using POC, which has already been implemented in actual fingerprint verification units [9]. We have also proposed iris recognition [10] and palmprint recognition [11] algorithms using POC. In this paper, we demonstrate that the same technique is also highly effective for recognizing dental radiographs. Experimental evaluation using a set of dental radiographs taken before and after dental treatment exhibits efficient identification performance of the

proposed system.

This paper is organized as follows: Sect. 2 presents an overview of the proposed dental radiograph identification system. Section 3 describes the phase-based image matching using POC. Section 4 descries a dental matching algorithm using POC. Section 5 presents a set of experiments for evaluating identification performance of the proposed algorithm. In Sect. 6, we end with some conclusions.

2. System Overview

We briefly describe the proposed dental radiograph identification system as shown in Fig. 2. The proposed system consists of three stages: (i) preprocessing, (ii) matching, and (iii) expert decision. In this system, the input images are the PM dental radiographs, and the registered images in the database are the AM dental radiographs. In the preprocessing stage (stage (i)), we enhance the contrast of the input image, since the radiograph images often contain the substantial noise. We assume that the registered images in the database have already been enhanced. In the matching stage (stage (ii)), we estimate the scale factor, rotation angle and translational displacement between the input image and the registered image, align the two images, and then calculate the similarity between the two images. The matching result is obtained as a list of few candidates, which is a ranking of the best matchings in the database. According to this list, the forensic experts make a final decision about the identity of the input image (stage (iii)).

The main part of the proposed system is the matching stage. The accurate matching algorithm makes possible to reduce identification tasks of forensic experts. In order to achieve accurate dental radiograph matching, we employ the high-accuracy image matching technique using Phase-Only Correlation (POC). This technique has been successfully applied to image registration and matching tasks for biometric authentication. In this system, the POC-based image matching technique is used to align two images and calculate the
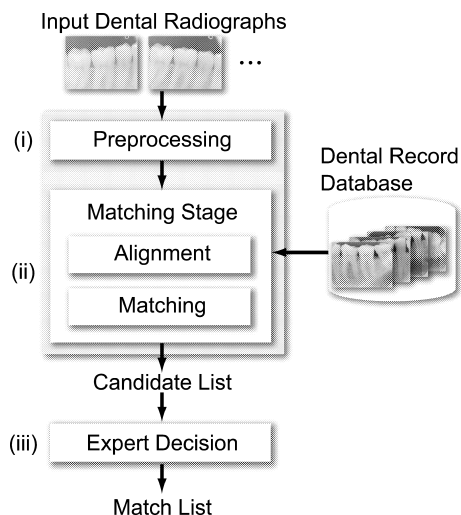

Fig. 2   Dental radiograph recognition system for human identification.

similarity between them.

3. Phase-Based Image Matching

3.1 Phase-Only Correlation Function

We introduce the principle of the POC function (which is sometimes called the "phase-correlation function") [5]–[7].

Consider two $N_1 \times N_2$ images, $f(n_1, n_2)$ and $g(n_1, n_2)$, where we assume that the index ranges are $n_1 = -M_1 \cdots M_1$ ($M_1 > 0$) and $n_2 = -M_2 \cdots M_2$ ($M_2 > 0$) for mathematical simplicity, and therefore $N_1 = 2M_1 + 1$ and $N_2 = 2M_2 + 1$. Let $F(k_1, k_2)$ and $G(k_1, k_2)$ denote the 2D DFTs of the two images. $F(k_1, k_2)$ and $G(k_1, k_2)$ are given by

$$
\begin{aligned}
F(k_1, k_2) &= \sum_{n_1=-M_1}^{M_1} \sum_{n_2=-M_2}^{M_2} f(n_1, n_2) W_{N_1}^{k_1 n_1} W_{N_2}^{k_2 n_2} \\
&= A_F(k_1, k_2) e^{j\theta_F(k_1, k_2)}, \tag{1}
\end{aligned}
$$

$$
\begin{aligned}
G(k_1, k_2) &= \sum_{n_1=-M_1}^{M_1} \sum_{n_2=-M_2}^{M_2} g(n_1, n_2) W_{N_1}^{k_1 n_1} W_{N_2}^{k_2 n_2} \\
&= A_G(k_1, k_2) e^{j\theta_G(k_1, k_2)}, \tag{2}
\end{aligned}
$$

where $k_1 = -M_1 \cdots M_1$, $k_2 = -M_2 \cdots M_2$, $W_{N_1} = e^{-j\frac{2\pi}{N_1}}$, and $W_{N_2} = e^{-j\frac{2\pi}{N_2}}$. $A_F(k_1, k_2)$ and $A_G(k_1, k_2)$ are amplitude components, and $\theta_F(k_1, k_2)$ and $\theta_G(k_1, k_2)$ are phase components. The cross-phase spectrum $R_{FG}(k_1, k_2)$ between $F(k_1, k_2)$ and $G(k_1, k_2)$ is given by

$$
R_{FG}(k_1, k_2) = \frac{F(k_1, k_2)\overline{G(k_1, k_2)}}{|F(k_1, k_2)\overline{G(k_1, k_2)}|} = e^{j\theta(k_1, k_2)}, \tag{3}
$$

where $\overline{G(k_1, k_2)}$ denotes the complex conjugate of $G(k_1, k_2)$ and $\theta(k_1, k_2)$ denotes the phase difference $\theta_F(k_1, k_2) - \theta_G(k_1, k_2)$. The POC function $r_{fg}(n_1, n_2)$ is 2D Inverse DFT of $R_{FG}(k_1, k_2)$ and is given by

$$
\begin{aligned}
r_{fg}(n_1, n_2) = &\frac{1}{N_1 N_2} \sum_{k_1=-M_1}^{M_1} \sum_{k_2=-M_2}^{M_2} R_{FG}(k_1, k_2) \\
&\times W_{N_1}^{-k_1 n_1} W_{N_2}^{-k_2 n_2}. \tag{4}
\end{aligned}
$$

When two images are similar, their POC function gives a distinct sharp peak. (When $f(n_1, n_2) = g(n_1, n_2)$, the POC function r_{fg} becomes the Kronecker delta function.) When two images are not similar, the peak drops significantly. The height of the peak can be used as a good similarity measure for image matching, and the location of the peak shows the translational displacement between the two images. Other important properties of POC used for biometric authentication tasks is that it is not influenced by image shift and brightness change, and it is highly robust against noise. See [8] for detailed discussions.

3.2 Band-Limited POC Function

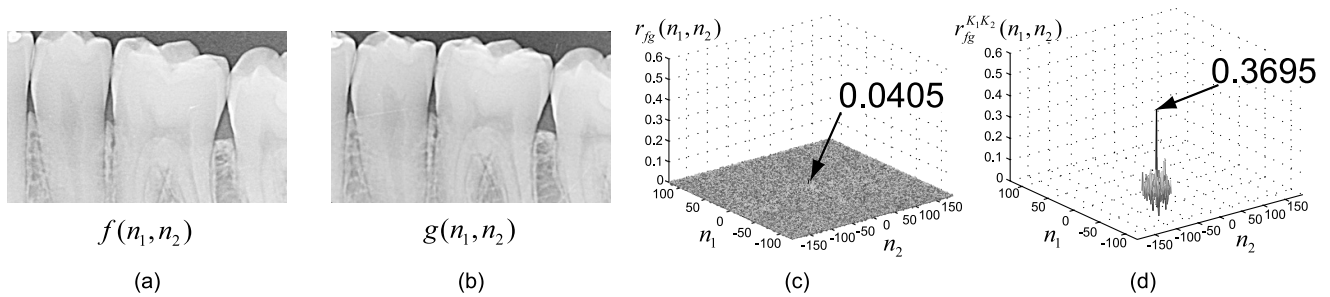We modify the definition of POC function to have a BLPOC

Fig. 3 Example of genuine matching using the original POC function and the BLPOC function: (a) input image $f(n_1, n_2)$, (b) registered image $g(n_1, n_2)$, (c) original POC function $r_{fg}(n_1, n_2)$, and (d) BLPOC function $r_{fg}^{K_1 K_2}(n_1, n_2)$ with $K_1/M_1 = K_2/M_2 = 0.1$.

Fig. 4 Example of impostor matching using the original POC function and the BLPOC function: (a) input image $f(n_1, n_2)$, (b) registered image $g(n_1, n_2)$, (c) original POC function $r_{fg}(n_1, n_2)$, and (d) BLPOC function $r_{fg}^{K_1 K_2}(n_1, n_2)$ with $K_1/M_1 = K_2/M_2 = 0.1$.
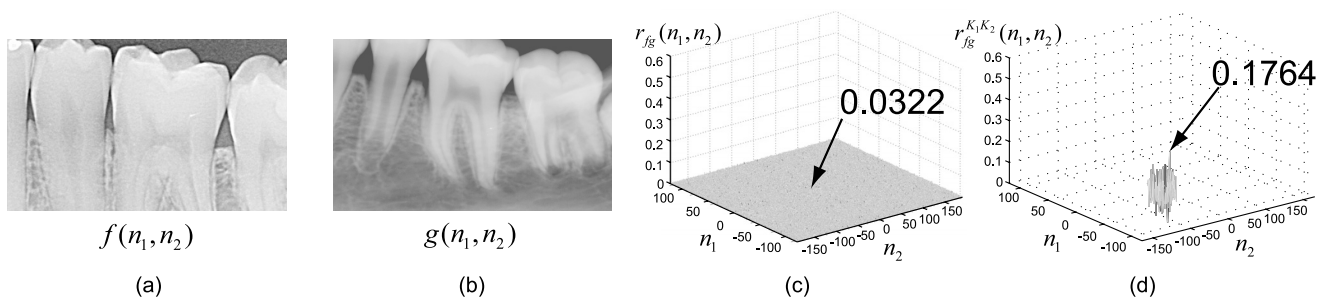
(Band-Limited Phase-Only Correlation) function dedicated to biometric authentication tasks. The idea to improve the matching performance is to eliminate meaningless high frequency components in the calculation of cross-phase spectrum $R_{FG}(k_1, k_2)$ depending on the inherent frequency components of images [8]. Assume that the ranges of the inherent frequency band are given by $k_1 = -K_1 \cdots K_1$ and $k_2 = -K_2 \cdots K_2$, where $0 \leq K_1 \leq M_1$ and $0 \leq K_2 \leq M_2$. Thus, the effective size of frequency spectrum is given by $L_1 = 2K_1 + 1$ and $L_2 = 2K_2 + 1$. The BLPOC function is given by

$$r_{fg}^{K_1 K_2}(n_1, n_2) = \frac{1}{L_1 L_2} \sum_{k_1 = -K_1}^{K_1} \sum_{k_2 = -K_2}^{K_2} R_{FG}(k_1, k_2)$$
$$\times W_{L_1}^{-k_1 n_1} W_{L_2}^{-k_2 n_2}, \qquad (5)$$

where $n_1 = -K_1 \cdots K_1$ and $n_2 = -K_2 \cdots K_2$. Note that the maximum value of the correlation peak of the BLPOC function is always normalized to 1 and does not depend on L_1 and L_2. Also, the translational displacement between the two images can be estimated by the correlation peak position.

Figures 3 and 4 show examples of genuine matching and impostor matching using the original POC function r_{fg} and the BLPOC function $r_{fg}^{K_1 K_2}$, respectively. The BLPOC function provides the higher correlation peak and better discrimination capability than the original POC function.

3.3 Scale Factor and Rotation Angle Estimation

The POC technique mentioned above can be extended to the registration for images including translation, rotation and scaling simultaneously [6]. We employ the log-polar mapping of the amplitude spectrum to transform the image scaling and rotation into image translation. The scale factor and rotation angle are estimated by detecting the corresponding translational displacements. We summarize the procedure for estimating the scale factor λ and the rotation angle θ as follows (see [6] for detailed discussions).

Input:
    the input image $f(n_1, n_2)$,
    the registered image $g(n_1, n_2)$.

Output:
    the relative rotation angle θ,
    the relative scale factor λ.

1. Calculate 2D DFTs of $f(n_1, n_2)$ and $g(n_1, n_2)$ to obtain $F(k_1, k_2)$ and $G(k_1, k_2)$.
2. Calculate amplitude spectra $|F(k_1, k_2)|$ and $|G(k_1, k_2)|$ (Fig. 5(b)). In general, most energy is concentrated in low-frequency domain. Hence, we use $\sqrt{|F(k_1, k_2)|}$ and $\sqrt{|G(k_1, k_2)|}$ instead of $|F(k_1, k_2)|$ and $|G(k_1, k_2)|$ (Fig. 5(c)).
3. Calculate the log-polar mappings $F_{LP}(l_1, l_2)$ and $G_{LP}(l_1, l_2)$ (Fig. 5(d)).
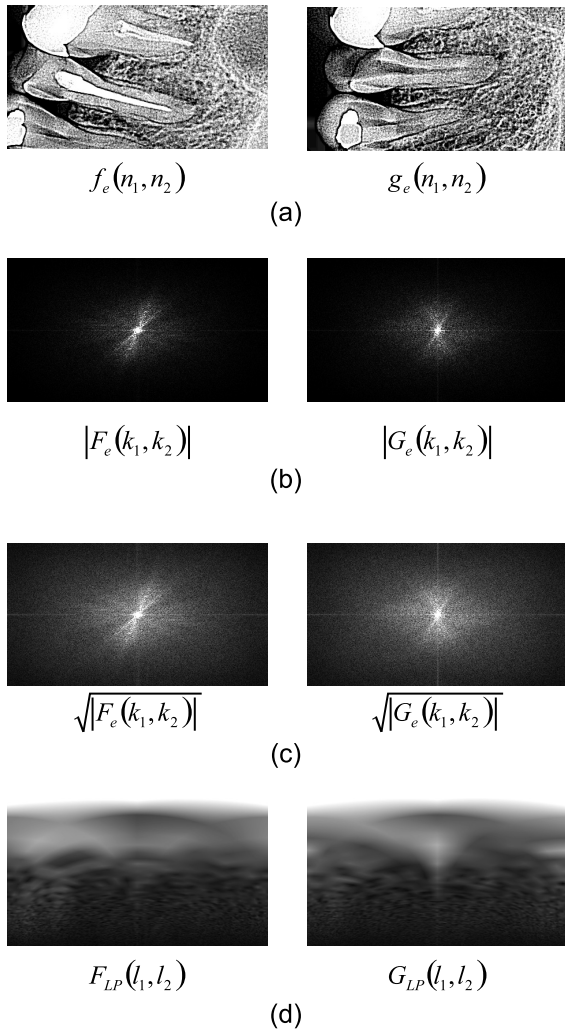4. Estimate the image displacement between $F_{LP}(l_1, l_2)$

$f_e(n_1, n_2)$ $g_e(n_1, n_2)$

(a)

$|F_e(k_1, k_2)|$ $|G_e(k_1, k_2)|$

(b)

$\sqrt{|F_e(k_1, k_2)|}$ $\sqrt{|G_e(k_1, k_2)|}$

(c)

$F_{LP}(l_1, l_2)$ $G_{LP}(l_1, l_2)$

(d)

Fig. 5 Scale factor and rotation angle estimation using POC: (a) the input image and the registered image after contrast enhancement, (b) amplitude spectra of the images, (c) square root of the amplitude spectra, and (d) log-polar mappings of the amplitude spectra.

and $G_{LP}(l_1, l_2)$ using the peak location of the BLPOC function $r_{F_{LP}G_{LP}}^{K_1 K_2}(n_1, n_2)$ to obtain λ and θ.

4. Dental Radiograph Matching Algorithm

In this section, we present a dental radiograph matching algorithm using POC. This algorithm corresponds to stages (i) and (ii) in Fig. 2. The proposed algorithm consists of four steps: (i) image enhancement, (ii) scaling, rotation and displacement alignment, (iii) common region extraction and (iv) matching as shown in Fig. 6. Figure 7 shows examples of dental radiograph matching using the proposed algorithm. We describe the details of each step as follows.

(i) Image enhancement

First step is to enhance radiograph images to allow accurate radiograph image processing, since these images are often blurred due to substantial noise and poor lighting. In our proposed algorithm, we improve the image quality by
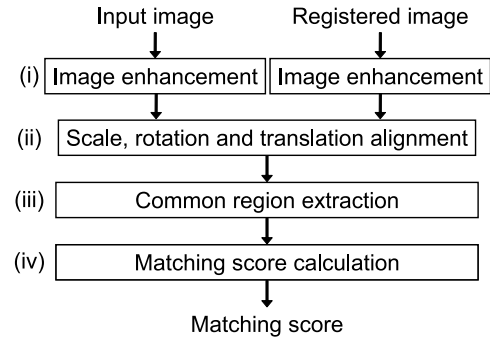

Fig. 6 Flow diagram of the proposed dental matching algorithm.

using local area contrast enhancement [12]. Let $f(n_1, n_2)$ be the input image. The enhanced image $f_e(n_1, n_2)$ is given by

$$f_e(n_1, n_2) = \frac{\nu \cdot m_f}{s_l(n_1, n_2)} \{f(n_1, n_2) - m_l(n_1, n_2)\} + m_l(n_1, n_2), \tag{6}$$

where ν is a constant, m_f is a global mean of $f(n_1, n_2)$, $m_l(n_1, n_2)$ is a local mean of $f(n_1, n_2)$, and $s_l(n_1, n_2)$ is a local variance of $f(n_1, n_2)$. In this paper, we employ $\nu = 0.5$. The global mean m_f is calculated as a global pixel mean for the entire image. The local mean $m_l(n_1, n_2)$ and variance $s_l(n_1, n_2)$ are calculated as a mean and variance for a 8×8 neighborhood about each pixel. Figure 7(b) shows the enhanced images, $f_e(n_1, n_2)$ and $g_e(n_1, n_2)$, of the input image $f(n_1, n_2)$ and the registered image $g(n_1, n_2)$, respectively. Note that the enhanced registered image $g_e(n_1, n_2)$ has already been in the database.

(ii) Scaling, rotation and displacement alignment

We need to normalize scaling, rotation and displacement between the enhanced input image $f_e(n_1, n_2)$ and the enhance registered image $g_e(n_1, n_2)$ in order to perform the high-accuracy dental radiograph matching. We estimate the scale factor λ and the rotation angle θ by using the technique described in Sect. 3.3. Using λ and θ, we obtain a scaling- and rotation-normalized image $g_{e\lambda\theta}(n_1, n_2)$ (Fig. 7(c)).

Then, we align the translational displacement between $f_e(n_1, n_2)$ and $g_{e\lambda\theta}(n_1, n_2)$ using the peak location of the BLPOC function $r_{f_e g_{e\lambda\theta}}^{K_1 K_2}(n_1, n_2)$. Thus, we have normalized versions of the registered image and the input image as shown in Fig. 7(d), which are denoted by $f'(n_1, n_2)$ and $g'(n_1, n_2)$.

(iii) Common region extraction

This step is to extract the overlapped region (intersection) of the two images $f'(n_1, n_2)$ and $g'(n_1, n_2)$. This process improves the accuracy of dental matching, since the non-overlapped areas of the two images become the uncorrelated noise components in the BLPOC function. In order to detect the effective areas in the registered image $f'(n_1, n_2)$ and the input image $g'(n_1, n_2)$, we examine the n_1-axis projection and the n_2-axis projection of pixel values. Only the common effective image areas, $f''(n_1, n_2)$ and $g''(n_1, n_2)$, with the same size are extracted for the succeeding image matching step (Fig. 7(e)).
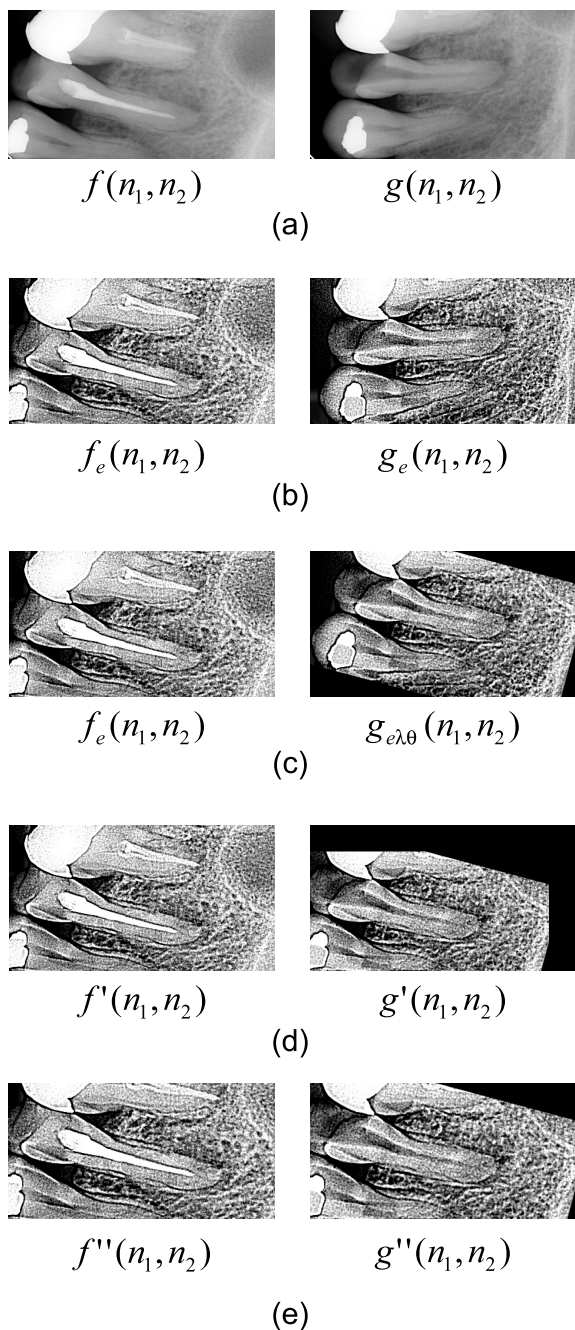
$f(n_1, n_2)$ $g(n_1, n_2)$

(a)

$f_e(n_1, n_2)$ $g_e(n_1, n_2)$

(b)

$f_e(n_1, n_2)$ $g_{e\lambda\theta}(n_1, n_2)$

(c)

$f'(n_1, n_2)$ $g'(n_1, n_2)$

(d)

$f''(n_1, n_2)$ $g''(n_1, n_2)$

(e)

Fig. 7 Example of dental radiograph matching using the proposed algorithm: (a) the input image and the registered image, (b) enhanced images, (c) scaling- and rotation-normalized images, (d) normalized images, and (e) extracted common regions.

(iv) Matching score calculation

We calculate the BLPOC function $r_{f''g''}^{K_1 K_2}(n_1, n_2)$ between the two extracted images $f''(n_1, n_2)$ and $g''(n_1, n_2)$, and evaluate the matching score. The matching score is given by the highest peak value of the BLPOC function $r_{f''g''}^{K_1 K_2}(n_1, n_2)$.

5. Experiments and Discussions

This section describes a set of experiments using a dental radiograph database for evaluating dental matching performance of the proposed system.

In practice, there are differences in dental structures between AM and PM dental radiographs. This is because the PM (or AM) radiographs may depict only a part of dental structures in the AM (or PM) radiographs, scaling and rotation may be present between AM and PM radiographs, and some teeth in PM radiograph may have been removed. Similar differences are also observed in dental radiographs taken before and after dental treatment. These differences occur because radiographs are taken by different radiologists at an interval of several weeks, and a damaged tooth may be removed and replaced by dental metal. In this experiment, we use dental radiographs taken before and after dental treatment instead of AM and PM dental radiographs. The dental radiographs taken before dental treatment are used as PM dental radiographs, while the dental radiographs taken after dental treatment are used as AM dental radiographs. Our dental radiograph database consists of 120 images (256×460 pixels) with 60 subjects and 2 different images of each dental radiograph.

Examples of dental radiographs used in experiments are shown in Fig. 8. The radiographs in Fig. 8(a) are taken in the process of crown restoration which is to remove portions of a damaged tooth and to bond a tooth-shaped covering in place. As shown in this figure, the damaged crown is replaced by the crown metal. The radiographs in Fig. 8(b) are taken in the process of root canal filling and under different lighting conditions. As shown in the left radiograph of this figure, the root filling material looks white on X-rays. The intersection area between radiographs in Fig. 8(c) is small, which may not provide sufficient information to identify whose radiograph it is. The radiographs in Fig. 8(d) are taken in the process of crown restoration and show a large degree of rotation when compared. The silhouette of the X-ray machine is also accidentally captured as shown in the right radiograph of this figure. Thus, using this test set, we evaluate performance of the matching algorithm under difficult conditions.

The performance of the identification system is evaluated by the Cumulative Match Curve (CMC), which illustrates the rank of the genuine pair against the recognition rate [13]. In order to generate a CMC, we first match each input image to all the registered images in the database, and then obtain the matching scores. In this experiment, the total number of matching pairs is 3,600 (=60×60). Next, the registered images are sorted by decreasing the matching scores for each input image. The input image is considered to be correctly recognized at the rank k if the registered image of the same person is among the first k images in the sorted registered images. The recognition rates for each rank are obtained as the probability that the input image is correctly recognized.
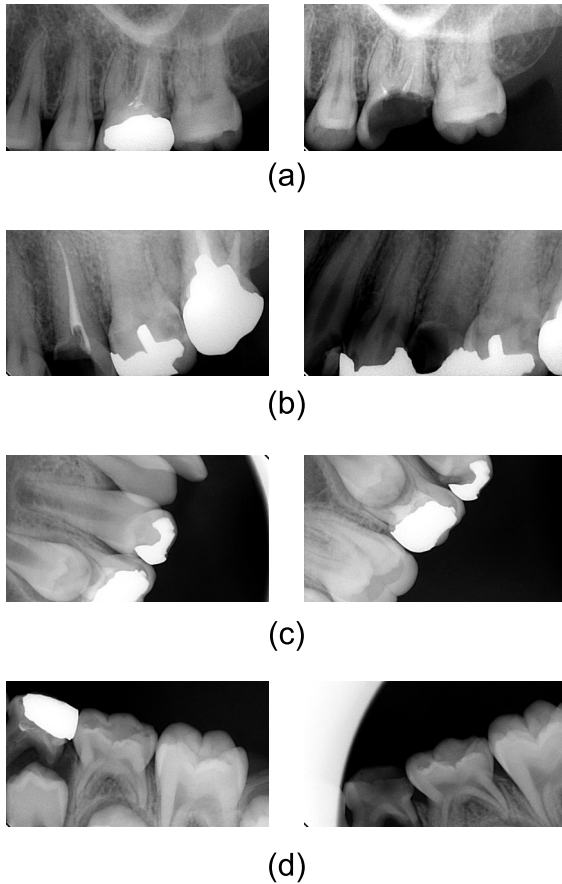
Fig. 8 Examples of dental radiographs used in experiments: the left-hand images are taken after dental treatment and the right-hand images are taken before dental treatment.
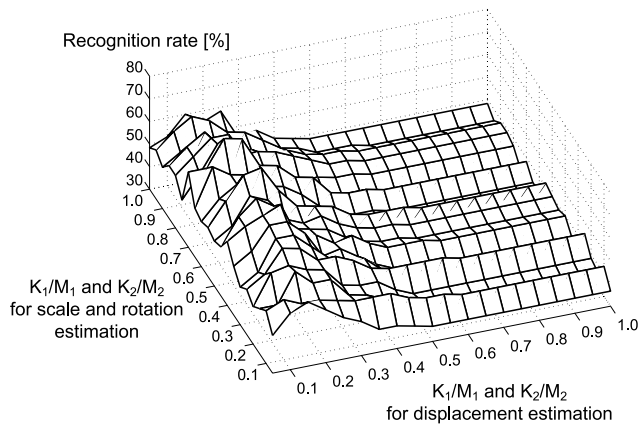

Fig. 9 Recognition rate when using top-1 radiograph, where K_1/M_1 and K_2/M_2 for scale, rotation and translation estimation are changed, and $K_1/M_1 = K_2/M_2 = 0.1$ for matching.

The performance of the proposed matching algorithm can be optimized by selecting the adequate value of the bandwidth parameters of BLPOC function K_1/M_1 and K_2/M_2. The parameters K_1/M_1 and K_2/M_2 are to be optimized in scaling and rotation alignment, displacement alignment and matching steps. In order to optimize matching per-
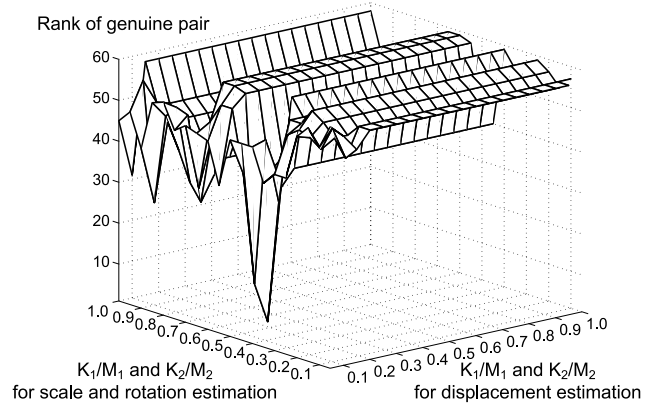

Fig. 10 Rank of the genuine pairs when reaching 100% recognition accuracy, where K_1/M_1 and K_2/M_2 for scale, rotation and translation estimation are changed, and $K_1/M_1 = K_2/M_2 = 0.1$ for matching.
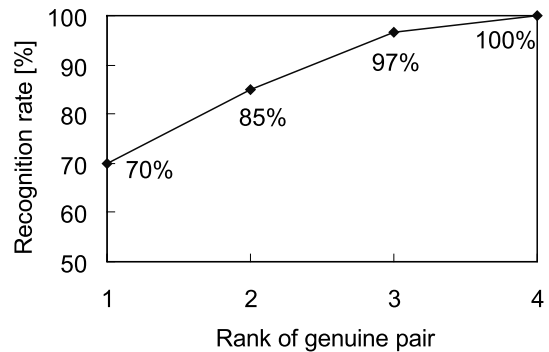

Fig. 11 Cumulative match curve of the proposed algorithm when using the optimal values of K_1/M_1 and K_2/M_2.

formance, the parameters K_1/M_1 and K_2/M_2 are changed from 0.05 to 1.00 for these three steps, where $K_1/M_1 = K_2/M_2$ for simplicity. Figures 9 and 10 show some examples of the experimental results. Figure 9 shows the recognition rate when using top-1 radiograph, where $K_1/M_1 = K_2/M_2 = 0.10$ for matching. Figure 10 shows the rank of the genuine pair when reaching 100% recognition accuracy, where $K_1/M_1 = K_2/M_2 = 0.10$ for matching. As a result, the optimal values of K_1/M_1 and K_2/M_2 are 0.45 for scaling and rotation alignment, 0.15 for displacement alignment, and 0.10 for matching. The parameters K_1/M_1 and K_2/M_2 for dental radiograph matching are smaller than those for other biometric matching. For example, the parameters of BLPOC function are $K_1/M_1 = 0.6$ and $K_2/M_2 = 0.2$ for iris matching [10] and $K_1/M_1 = K_2/M_2 = 0.75$ for palmprint matching [11], respectively. This means that the important phase information for dental radiograph matching are concentrated in lower frequency domain than that for iris matching and palmprint matching. Thus, we need to design the BLPOC function depending on each biometric technique in order to achieve accurate matching.

Figure 11 shows the CMC of the proposed algorithm using the optimal values of K_1/M_1 and K_2/M_2. Using the top-1 radiograph, the recognition accuracy is 70% (=42/60).

$$f(n_1, n_2)$$

(a)

$$g(n_1, n_2)$$

(b)

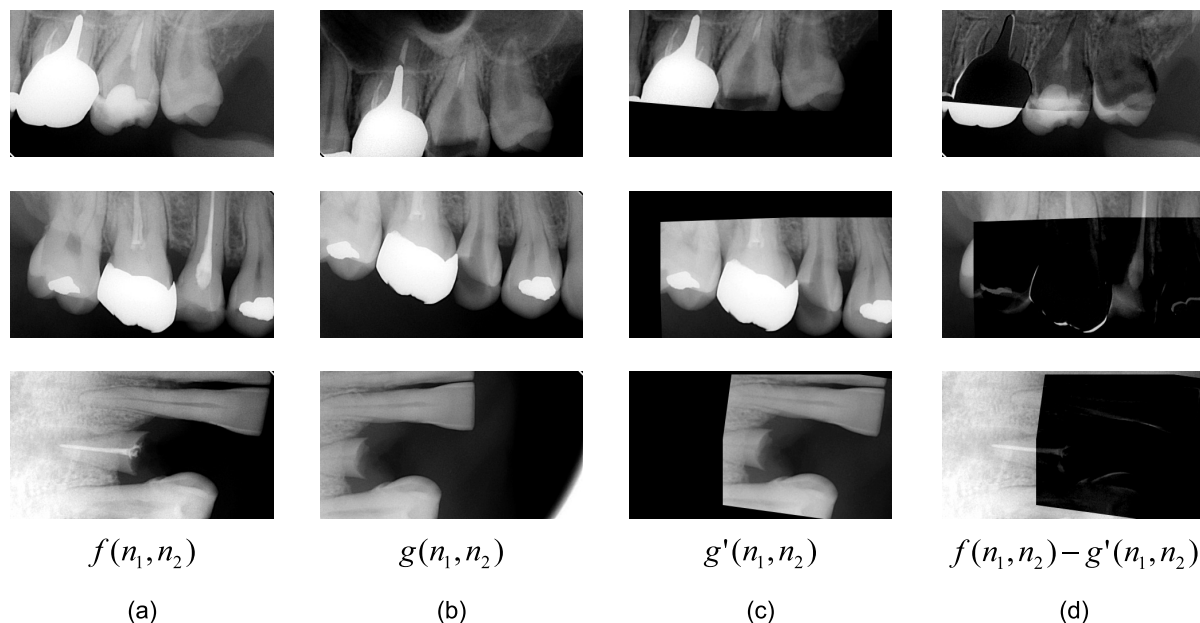$$g'(n_1, n_2)$$

(c)

$$f(n_1, n_2) - g'(n_1, n_2)$$

(d)

Fig. 12 Examples of the registration result of dental radiographs: (a) the input image $f(n_1, n_2)$, (b) the registered image $g(n_1, n_2)$, (c) the scale-, rotation- and displacement-normalized image, $g'(n_1, n_2)$, and (d) the subtraction image between (a) and (c).

The recognition accuracy reaches 100% when the top-4 radiographs are used. As a result, by using the proposed algorithm, the number of radiograph pairs to be checked by forensic experts can be reduced to 6.7% (=240/3,600) for all the pairs. The computation time is 2.0 seconds, where MATLAB 6.5.1 on Pentium4 3.0 GHz is used. Thus, the total computation time of this experiment is 2 hours. Although further analysis using a larger database is required for evaluating the system, this experiment demonstrates a potential capability of the proposed system to identify dental radiographs.

Figure 12 shows the examples of the registration result between the input and registered images. Figure 12(d) indicates that the subtraction images between aligned radiographs clearly show the dental work. It is expected that we can support the dental treatment by using the proposed matching algorithm.

As is observed in these experimental results, the proposed algorithm is useful for matching low-quality dental radiographs.

6. Conclusion

This paper has presented a dental radiograph recognition system using Phase-Only Correlation (POC) for human identification. Experimental evaluation demonstrates efficient performance of our proposed system for low-quality dental radiographs. For our future works, we will improve performance of a dental radiograph identification system and evaluate performance of the developed system using a large-scale database of AM and PM dental radiographs. We will also develop a Computer-Aided Diagnosis (CAD) system using POC for accurate assessment and treatment of dental diseases.

References

[1] A. Jain, A. Ross, and S. Pankanti, "Biometrics: A tool for information security," IEEE Trans. Information Forensics and Security, vol.1, no.2, pp.125–143, June 2006.

[2] H. Chen and A.K. Jain, "Dental biometrics: Alignment and matching of dental radiographs," IEEE Trans. Pattern Anal. Mach. Intell., vol.27, no.8, pp.1319–1326, Aug. 2005.

[3] G. Fahmy, D. Nassar, E. Haj-Said, H. Chen, O. Nomir, J. Zhou, R. Howell, H.H. Ammar, M. Abdel-Mottaleb, and A.K. Jain, "Toward an automated dental identification system," J. Electronic Imaging, vol.14, no.4, pp.043018-1–043018-13, Oct. 2005.

[4] A.K. Jain and H. Chen, "Matching of dental X-ray images for human identification," Pattern Recognit., vol.37, no.7, pp.1519–1532, July 2004.

[5] C.D. Kuglin and D.C. Hines, "The phase correlation image alignment method," Proc. Int. Conf. Cybernetics and Society, pp.163–165, 1975.

[6] K. Takita, T. Aoki, Y. Sasaki, T. Higuchi, and K. Kobayashi, "High-accuracy subpixel image registration based on phase-only correlation," IEICE Trans. Fundamentals, vol.E86-A, no.8, pp.1925–1934, Aug. 2003.

[7] K. Takita, M.A. Muquit, T. Aoki, and T. Higuchi, "A sub-pixel correspondence search technique for computer vision applications," IEICE Trans. Fundamentals, vol.E87-A, no.8, pp.1913–1923, Aug. 2004.

[8] K. Ito, H. Nakajima, K. Kobayashi, T. Aoki, and T. Higuchi, "A fingerprint matching algorithm using phase-only correlation," IEICE Trans. Fundamentals, vol.E87-A, no.3, pp.682–691, March 2004.

[9] http://www.aoki.ecei.tohoku.ac.jp/research/poc.html, Products using phase-based image matching

[10] K. Miyazawa, K. Ito, T. Aoki, K. Kobayashi, and H. Nakajima, "A phase-based iris recognition algorithm," Lecture Notes in Computer Science (ICB2006), vol.3832, pp.356–365, Dec. 2005.

[11] K. Ito, T. Aoki, H. Nakajima, K. Kobayashi, and T. Higuchi, "A

palmprint recognition algorithm using phase-based image matching," Proc. 2006 IEEE Int. Conf. Image Processing, pp.2669–2672, Oct. 2006.

[12] G.X. Ritter and J.N. Wilson, Handbook of Computer Vision Algorithms in Image Algebra, CRC Press, 1996.

[13] R.M. Bolle, J.H. Connell, S. Pankanti, N.K. Ratha, and A.W. Senior, Guide to Biometrics, Springer, 2004.

Eiko Kosuge received the D.D.S. degree, and the Ph.D. degree from Kanagawa Dental College, Yokosuka, Japan, in 1996 and 2005, respectively. She is currently a Lecturer of Kanagawa Dental College. Her research interest includes biomedical image processing and dental radiograph identification systems.

Ryota Kawamata received the D.D.S. degree from Nihon University Dental School, Matsudo, Japan, in 1995. He is currently an Assistant Professor of Kanagawa Dental College, Yokosuka, Japan. His research interest includes nonlinear digital signal processing, computer graphics and biomedical image processing.

Isamu Kashima received the D.D.S. degree, and Ph.D. degree from Kanagawa Dental College, Yokosuka, Japan, in 1975 and 1979, respectively. He is currently a Professor and has been Associate Dean from 2005 at Kanagawa Dental College. His research interests include development of evaluating therapeutic effect with osteoporosis. Dr. Kashima received the Scientific Merit from RSNA in 1996.

Koichi Ito received the B.E. degree in electronic engineering, and the M.S. and Ph.D. degree in information sciences from Tohoku University, Sendai, Japan, in 2000, 2002 and 2005, respectively. He is currently a Research Associate of the Graduate School of Information Sciences at Tohoku University. From 2004 to 2005, he was a Research Fellow of the Japan Society for the Promotion of Science. His research interest includes signal and image processing, and biometric authentication.
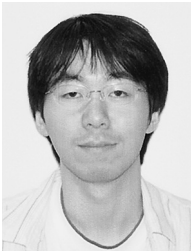
Akira Nikaido received the B.E. degree in information engineering from Tohoku University, Sendai, Japan, in 2006. He is currently working toward the M.S. degree of the Graduate School of Information Sciences at Tohoku University. His research interest includes signal and image processing, and biometric authentication.

Takafumi Aoki received the B.E., M.E., and D.E. degrees in electronic engineering from Tohoku University, Sendai, Japan, in 1988, 1990, and 1992, respectively. He is currently a Professor of the Graduate School of Information Sciences at Tohoku University. For 1997–1999, he also joined the PRESTO project, Japan Science and Technology Corporation (JST). His research interests include theoretical aspects of computation, VLSI computing structures for signal and image processing, multiple-valued logic, and biomolecular computing. Dr. Aoki received the Outstanding Paper Award at the 1990, 2000, 2001 and 2006 IEEE International Symposiums on Multiple-Valued Logic, the Outstanding Transactions Paper Award from the Institute of Electronics, Information and Communication Engineers (IEICE) of Japan in 1989 and 1997, the IEE Ambrose Fleming Premium Award in 1994, the IEICE Inose Award in 1997, the IEE Mountbatten Premium Award in 1999, and the Best Paper Award at the 1999 IEEE International Symposium on Intelligent Signal Processing and Communication Systems.